Aluminum Metasurface With Hybrid Multipolar Plasmons for 1000-Fold Broadband Visible Fluorescence Enhancement and Multiplexed Biosensing

Radwanul Hasan Siddique[1,3†], Shailabh Kumar[1,†], Vinayak Narasimhan[1], Hyounghan Kwon[1], and Hyuck Choo[1,2,3*]

[1]Department of Medical Engineering, California Institute of Technology, 1200 E. California Blvd., MC 136-93, Pasadena, California 91125, USA.

[2]Department of Electrical Engineering, California Institute of Technology, 1200 E. California Blvd., MC 136-93, Pasadena, California 91125, USA.

[3]Samsung Advanced Institute of Technologies, Samsung Electronics, 130 Samseong-ro, Maetan-dong, Yeongtong-gu, Suwon, Gyeonggi-do, 16678, South Korea.

[†]These authors contributed equally to this work.

[*]E-mail: hyuck.choo@samsung.com; hchoo@caltech.edu

Supplementary Information

Section S1: Enhancement factors

S1.1 Enhancement factor calculations

Experimental fluorescence enhancement factors were calculated by comparing the ratio of molecular fluorescence obtained from diffusing molecules on the nDISC regions as compared to on a control non-enhancing substrate. Using the equation:[1-2]

$$EF = \frac{I1 \times N2}{I2 \times N1}$$

Where I1 is the integrated fluorescence intensity from N1 number of molecules at the nDISC region, and I2 is the total fluorescence intensity from N2 number of molecules on a nontextured glass surface. Since, the same concentration of molecules was added to both substrates, we assume the volumetric density of molecules, η. Then the number of molecules near the hotspot for the nDISC surfaces can be represented as: $N1 = \eta \times V1$ where V1 is the effective hotspot volume at the dielectric between Al layers. FDTD simulations were consulted to calculate an effective distance from the hotspot where the molecule can experience a significant electromagnetic field enhancement. An effective distance of 25 nm and dielectric thickness of 5 nm were used. For the nonstructured control surface, number of molecules can be represented as $N2 = \eta \times V2$, where V2 is the confocal volume near a flat surface used as control. The effective focal depth of field for the microscope and the substrate was estimated as 0.285 μm. Fluorescence intensities I1 and I2 were obtained from the images after background subtraction. Average intensities were calculated around the hotspots for I1 and over control surfaces for I2, for EF calculation.

S1.2 Normalized Enhancement factor: The quantum yield (QE) enhancements were calculated at the respective wavelengths for the three fluorophores using the equation:[3]

$$\eta = \frac{\frac{\gamma_r}{\gamma_0}}{(1 - \eta_0) + \frac{\gamma_r}{\gamma_0} + \frac{\gamma_{nr}}{\gamma_0}}$$

These calculated QE enhancements are shown in table S1 and were used to normalize the absolute enhancement factors calculated previously. The normalized EF is thus independent of any quantum yield enhancement and solely represents localized electromagnetic and molecular enhancement at the hotspot.

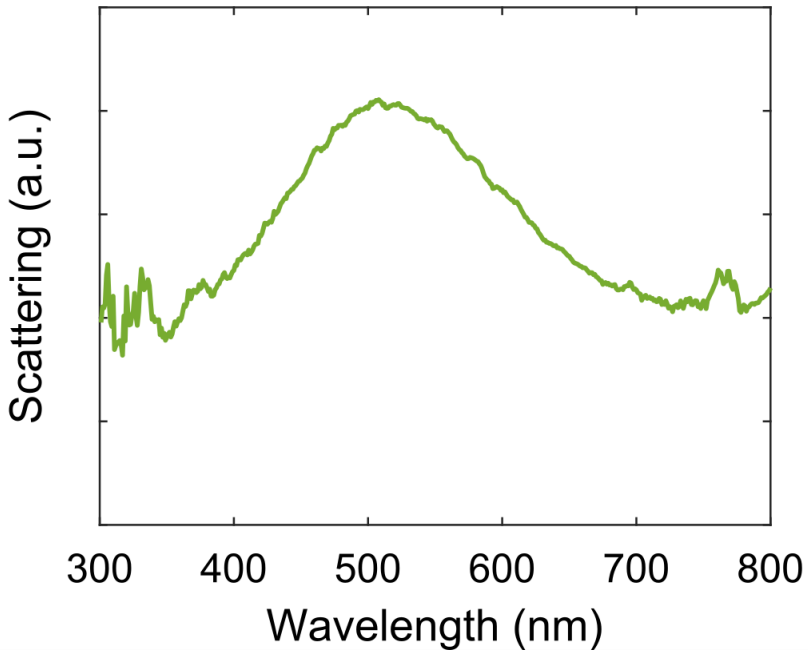

Figure S1. Experimental scattering of nDISC nanoantenna. Dark field scattering measurement of FIB-milled 500 nm nDISC antenna shows a scattering peak at 507 nm with a quality factor of 4.15.

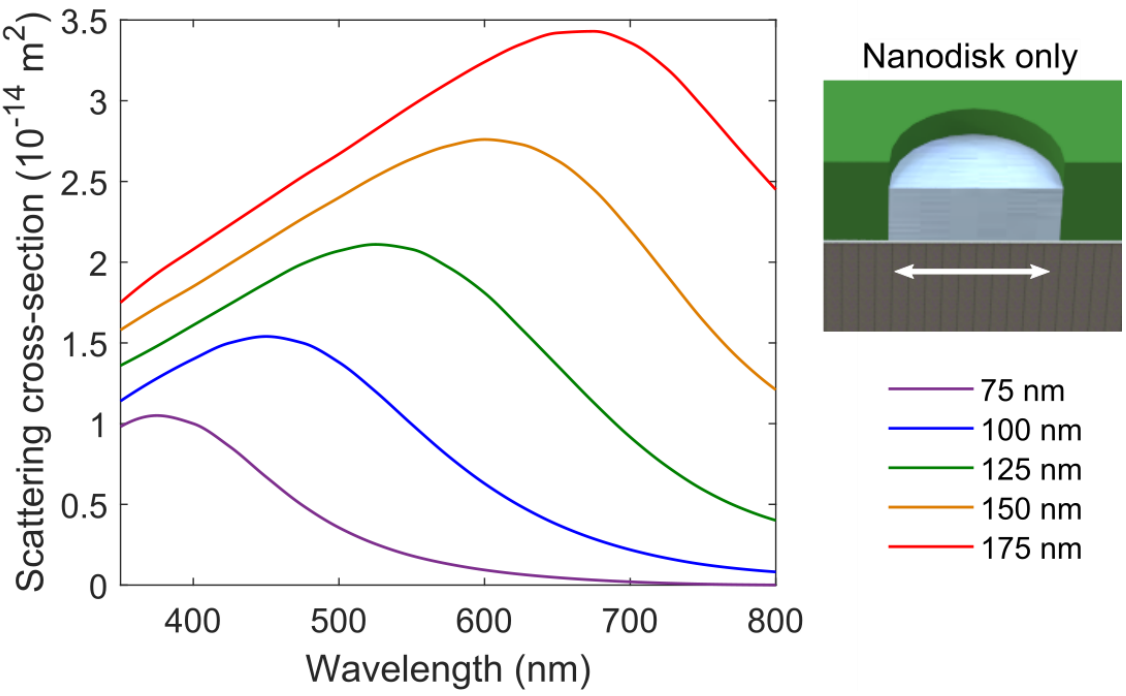

Figure S2. Simulated scattering spectra of lone Al nanodisks inside a dielectric cavity.

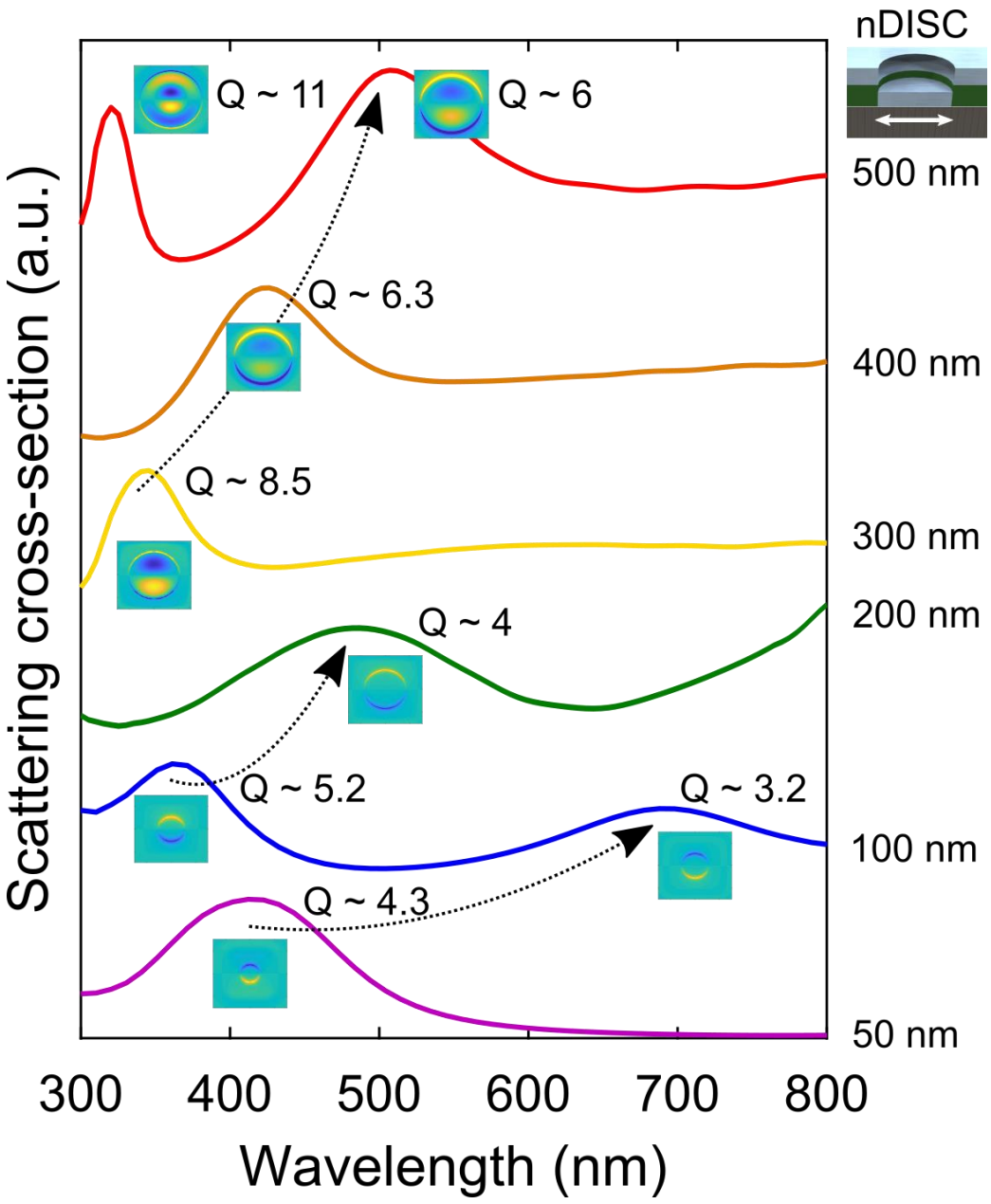

Figure S3. Simulated scattering of Al nDISC nanoantenna with different diameter. Calculated quality factors of hybrid multipolar scattering peaks and their corresponding out-of-plane field component E_z show the superior plasmon properties of larger nDISC nanoantenna.

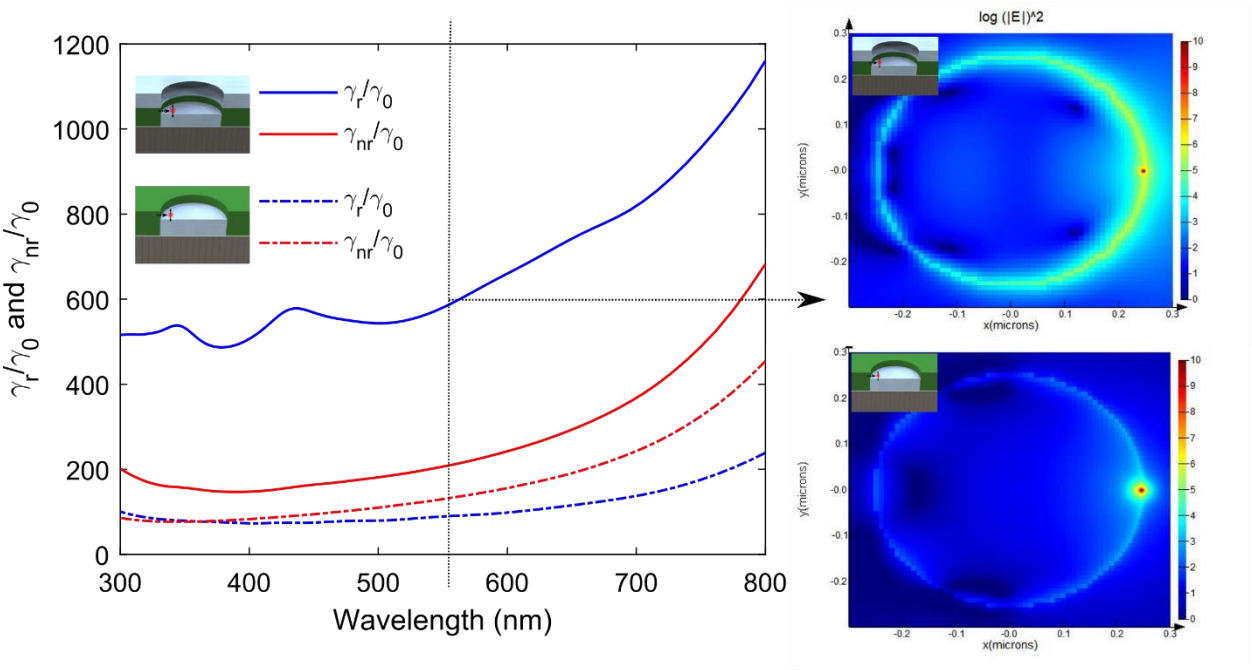

Figure S4. FDTD Simulation of radiative and non-radiative enhancements spectra for a dipole placed 2.5 nm above the metal disk and 2.5 nm to the side in a 500 nm Al nDISC and nanodisk. nDISC shows almost threefold increase in the radiative enhancement over non-radiative enhancement. Whereas, radiative enhancements of nanodisk is largely dominated by non-radiative enhancements demonstrating nanodisk's poor performance on dipole's emission enhancement. Simulations of emission profiles of a dipole on both plasmonic Al nDISC and single nanodisk antennae at emission wavelength of 568 nm is shown in the right panel confirming the enhanced coupling of emitter's radiation to LDOS modes of nDISC.

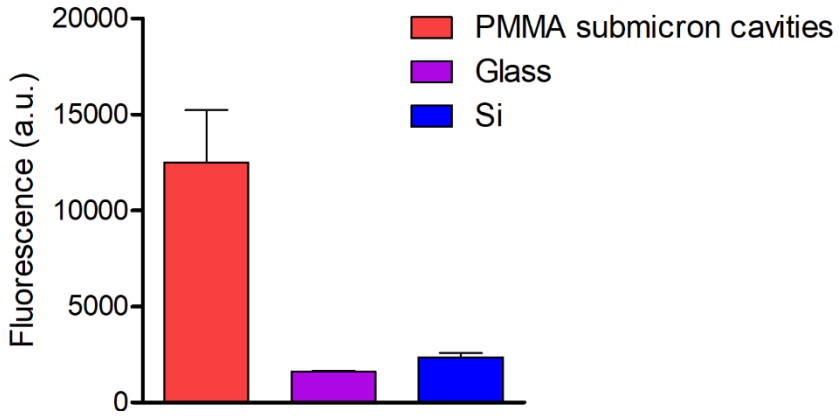

Figure S5. DNA adsorption on fabricated PMMA vs silica. Cy3-tagged aptamers were added to PMMA submicron cavities prepared using the phase-separation method, standard glass slides and silicon pieces with native SiO_2. Higher fluorescence intensity was observed on PMMA substrates indicating enhanced surface adhesion of the diffusing single-stranded DNA.

Fluorophore	QE enhancement
FAM	0.831
Cy3	7.282
Cy5	2.620

Table S1. Quantum efficiency enhancement calculated at the respective excitation wavelengths for three fluorophores on the nDISC nanoantenna metasurface.

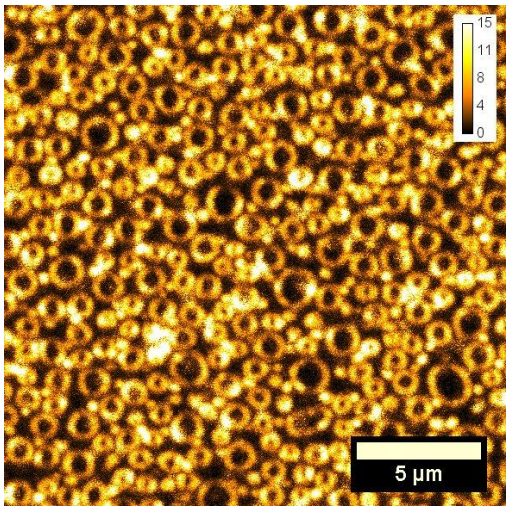

Figure S6. Figure shows normalized fluorescence image of a nDISC with PMMA nanoring with respect to a PMMA submicron cavity surface (DNA tagged with FAM). The color bar represents the raw intensity enhancement of the nDISC with respect to the PMMA submicron cavities.

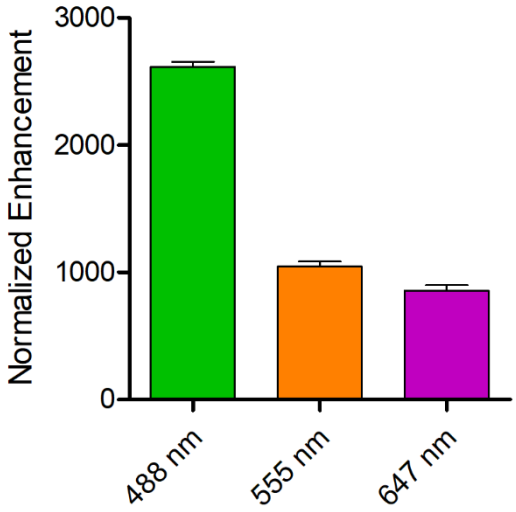

Figure S7. Normalized broadband enhancement factors. Enhancement of fluorescence normalized with respect to dye quantum yield for three visible wavelengths on the Al nDISC substrate with PMMA nanoring. This factor eliminates the effect of varying fluorophore quantum efficiencies. Electromagnetic field enhancement and enhanced molecular capture due to the PMMA nanoring as compared to control glass slide substrates are taken into account.

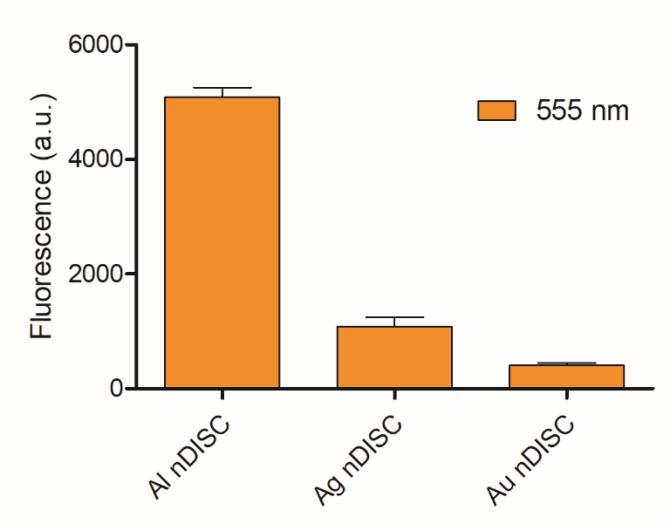

Figure S8. Fluorescence comparison of nDISC nanoantenna metasurfaces with different metals. Fluorescence response of nDISC metasurfaces without any change in substrate geometry, while changing the metal using Cy3-tagged aptamers.

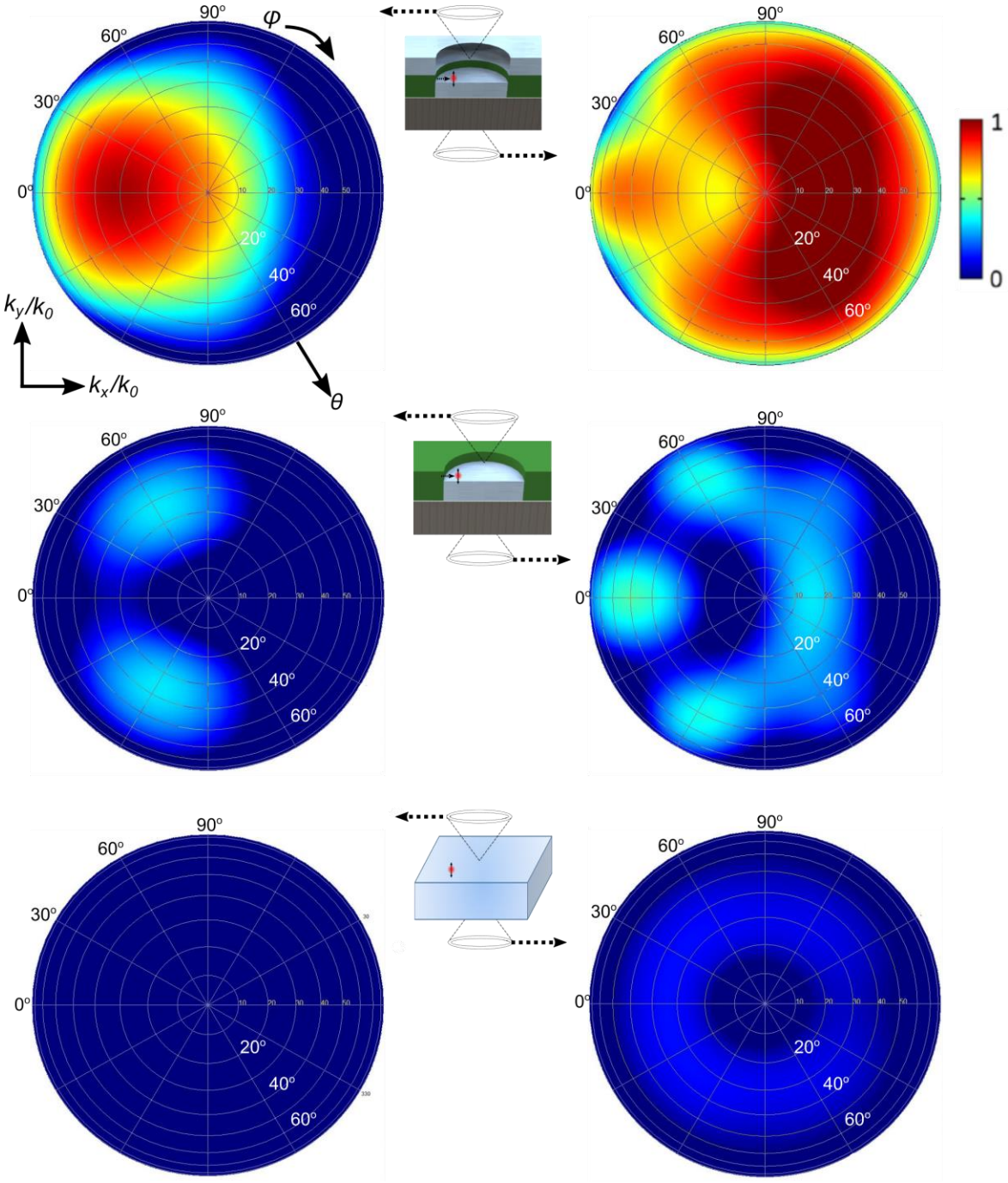

Figure S9. Emission intensity in the direction (θ, φ) for emission into the back-ward half-space (left) and into the forward substrate half-space (right) from the electric dipole inside nDISC cavity (top), on single Al nanodisk (middle) and on the flat glass (bottom). All calculated far-field patterns are normalized with respect to the same global maximum emission.

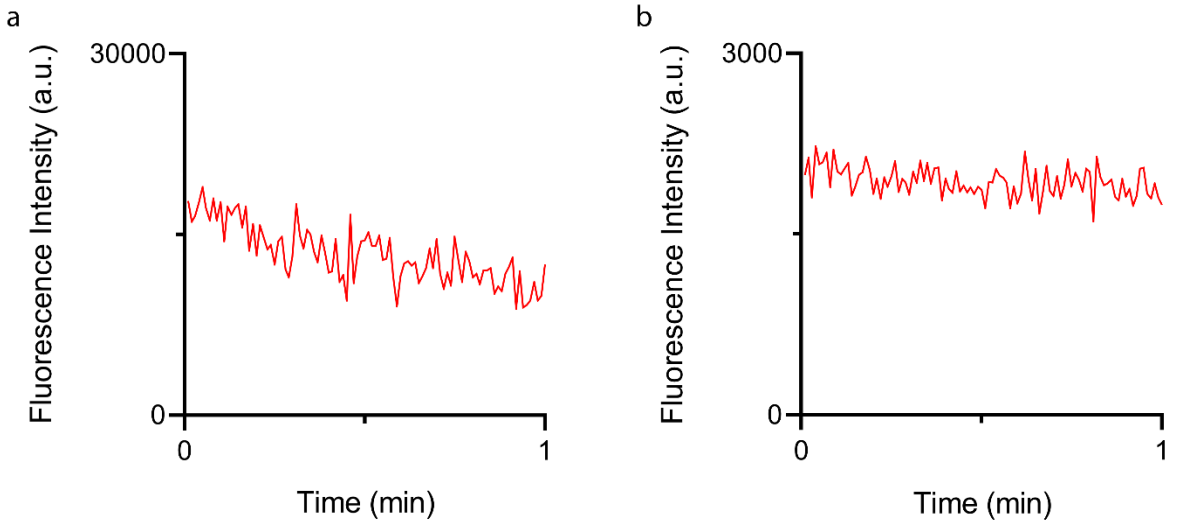

Figure S10. Time-lapse analysis of mean fluorescence obtained from a single nDISC at two different concentrations (a) 1 µM and (b) 10 nM. At high concentrations, we see higher intensity but also photobleaching of the signal over time, indicating that molecules are already bound on the PMMA nanoring surface. At 100-fold lower concentration, we do not observe decrease in signal over time, indicating that the photobleaching is countered by arrival of unbound molecules or most of the signal is from yet unbound molecules diffusing near the hotspot.

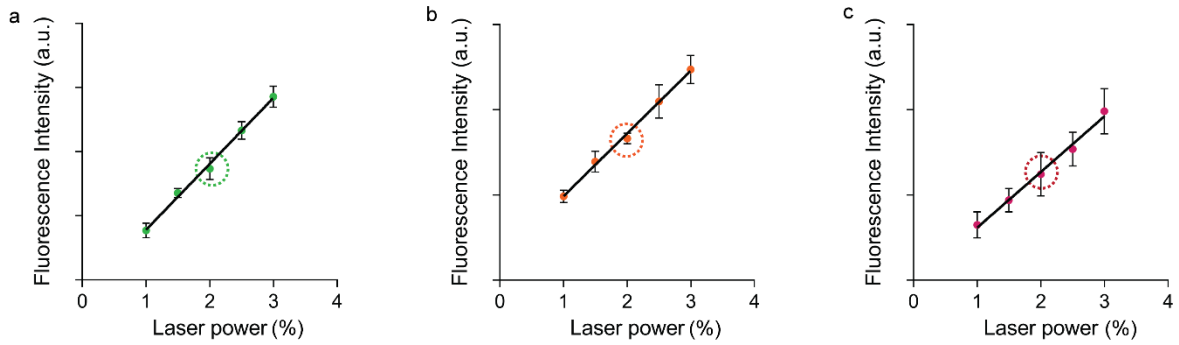

Figure S11. Plot showing obtained fluorescence from fluorophore-linked aptamers (1 µM) for laser powers ranging from 1-3% and fluorophores including (a) FAM (b) Cy3 and (c) Cy5. We used 2% laser power for all the measurements made in the manuscript (FAM and Cy3 - 0.2 mW, Cy5 - 0.1 mW). The results indicate a linear response between laser power and fluorophores in the target range.

References:

1. Cai, W.; Ren, B.; Li, X.; She, C.; Liu, F.; Cai, X.; Tian, Z.-Q., Investigation of Surface-Enhanced Raman Scattering from Platinum Electrodes using a Confocal Raman Microscope: Dependence of Surface Roughening Pretreatment. *Surf. Sci.* **1998,** *406*, 9-22.

2. Smythe, E. J.; Dickey, M. D.; Bao, J.; Whitesides, G. M.; Capasso, F., Optical Antenna Arrays on a Fiber Facet for *In Situ* Surface-Enhanced Raman Scattering Detection. *Nano Lett.* **2009,** *9*, 1132-1138.
3. Mack, D. L.; Cortés, E.; Giannini, V.; Török, P.; Roschuk, T.; Maier, S. A., Decoupling Absorption and Emission Processes in Super-Resolution Localization of Emitters in a Plasmonic Hotspot. *Nat. Commun.* **2017,** *8*, 14513.